Metal–Metal Interactions

Deutsche Ausgabe: DOI: 10.1002/ange.201509412
Internationale Ausgabe: DOI: 10.1002/anie.201509412

Metal–Metal Interactions in Heterobimetallic Complexes with Dinucleating Redox-Active Ligands

*Daniël L. J. Broere, Dieuwertje K. Modder[+], Eva Blokker[+], Maxime A. Siegler, and Jarl Ivar van der Vlugt**

Dedicated to Professor Franc Meyer on the occasion of his 50th birthday

Abstract: *The tuning of metal–metal interactions in multinuclear assemblies is a challenge. Selective P coordination of a redox-active PNO ligand to Au^{I} followed by homoleptic metalation of the NO pocket with Ni^{II} affords a unique trinuclear Au–Ni–Au complex. This species features two antiferromagnetically coupled ligand-centered radicals and a double intramolecular d^8–d^{10} interaction, as supported by spectroscopic, single-crystal X-ray diffraction, and computational data. A corresponding cationic dinuclear Au–Ni analogue with a stronger d^8–d^{10} interaction is also reported. Although both heterobimetallic structures display rich electrochemistry, only the trinuclear Au–Ni–Au complex facilitates electrocatalytic C–X bond activation of alkyl halides in its doubly reduced state. Hence, the presence of a redox-active ligand framework, an available coordination site at gold, and the nature of the nickel–gold interaction appear to be essential for this reactivity.*

The ability of transition metals to change their oxidation state is one of the cornerstones of organometallic catalysis.[1] The redox potential (as well as other types of reactivity) of a complex may be altered by the coordination of different spectator ligands, although this tuning is typically limited. The strategy of employing redox-active ligands in the coordination sphere of transition metals continues to attract much interest.[2] These systems generally span a much wider redox-potential range than complexes with spectator ligands and thus offer more versatile and modular reactivity with a specific transition-metal complex, thereby creating new opportunities for electron transfer to or from coordinated substrates. Redox-active ligands have initially been utilized primarily to induce two-electron transformations at metal centers that are redox-inert, prone to undergo one-electron processes, or that are lacking d electrons to induce two-electron bond activation processes.[3] In contrast, we recently disclosed radical reactivity with square-planar Pd^{II} complexes mediated by redox-active ligand-to-substrate single electron transfer.[4]

Synthetic systems featuring metal–metal interactions have successfully been exploited to facilitate (multi-electron) chemical transformations.[5] In the case of heterobimetallic architectures, the electronegativity difference between the metals can lead to polarized $M1^{\delta-}$–$M2^{\delta+}$ bonding, enabling the generation of reactive intermediates by charge transfer between metals.[6] Alternatively, electron repulsion between two electron-rich elements can destabilize a reduced state, thereby inducing reactivity.[7] Combining redox-active ligand chemistry with heterodinuclear metal–metal interactions could enable new modes of electronic communication that may enable new pathways for substrate conversion. Homoleptic complexes, $M(L^{isq^-})_2$, of square-planar d^8 metal centers featuring the iminosemiquinone (isq^-) form of redox-active amidophenolate type ligands are well-known, and their electrochemical and spectroscopic properties have been studied in great detail.[8] However, heterobimetallic architectures featuring a homoleptic $M(L^{isq^-})_2$ core structure are unknown to the best of our knowledge. The introduction of a second metal in close proximity to the metal bearing the redox-active ligand may allow for a tunable metal–metal interaction through a ligand-based redox stimulus (Figure 1).

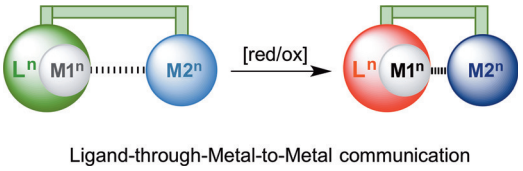

Figure 1. Ligand-through-metal-to-metal communication induced by a ligand-based redox process.

To address this challenge, we envisioned that the recently reported PNO ligand **1**[4] could be used for the targeted synthesis of well-defined (hetero)bimetallic complexes. Selective initial monodentate coordination of the "soft" phosphine donor to M1 would create a metalloligand that could incorporate a second metal, M2, in the "hard" NO pocket. Anticipating the preferred formation of a homoleptic coordination mode around M2, this could provide well-defined M1–M2–M1 architectures with the potential for intramolec-

[*] D. L. J. Broere, D. K. Modder,[+] E. Blokker,[+] Dr. ir. J. I. van der Vlugt
van 't Hoff Institute for Molecular Sciences
University of Amsterdam
Science Park 904, 1098 XH Amsterdam (The Netherlands)
E-mail: j.i.vandervlugt@uva.nl
Homepage: http://www.homkat.nl
Dr. M. A. Siegler
Department of Chemistry, John Hopkins University
3400 N, Charles St., Baltimore, MD 21218 (USA)
[+] These authors contributed equally to this work.

Supporting information for this article is available on the WWW under http://dx.doi.org/10.1002/anie.201509412.

ular metal–metal interactions. Herein, we report the synthesis, characterization, and initial reactivity of the unique trinuclear Au_2Ni complex **3**, which features two intramolecular d^8–d^{10} interactions and is held together by the presence of two redox-active ligands. We also describe the cationic dinuclear AuNi derivative **4**, which exhibits an even more pronounced d^8–d^{10} interaction. Both complexes undergo several ligand-based redox events in cyclic voltammetry. DFT calculations have provided insight into the electronic interactions between Ni and Au. Ligand-centered two-electron reduction of complex **3** generates an electrocatalyst for the C–X bond activation of alkyl halides, with subsequent C–C bond formation. The presence of all three components (gold, nickel, and redox-active ligand) appears to be essential for the observed reactivity, as confirmed by control experiments. This discovery paves the way to novel multimetallic design principles based on redox-active ligand-through-metal-to-metal electronic communication and non-traditional reactivity with transition metals.

Treatment of PNO ligand **1** (^{31}P NMR: $\delta = -20.25$ ppm) with $AuCl(SMe_2)$ afforded complex **2** (^{31}P NMR: $\delta =$ 19.97 ppm) in near-quantitative yield (Scheme 1). Layering

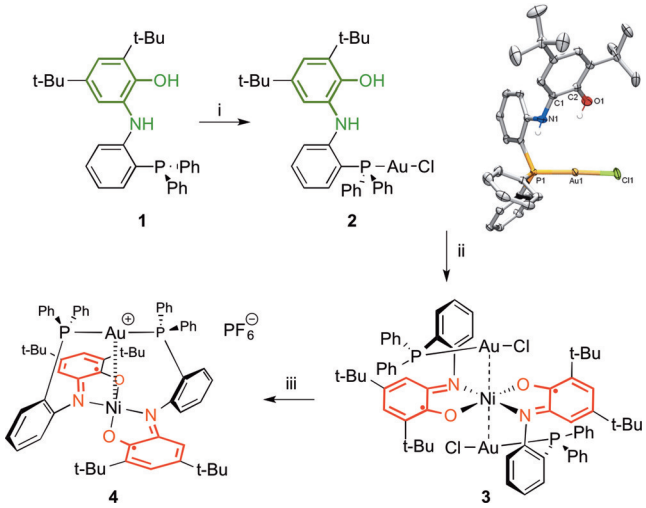

Scheme 1. Synthesis of complexes **2**–**4** starting from ligand **1**. Reagents and conditions: i) $AuClSMe_2$, CH_2Cl_2; ii) $Ni(NO_3)_2{\cdot}6H_2O$, NEt_3, air, MeCN; iii) $TlPF_6$, MeCN.

a solution of **2** in chloroform with pentane afforded colorless single crystals (see Scheme 1). In the solid state, complex **2** shows a slightly distorted linear coordination geometry with a P1-Au1-Cl1 angle of 176.84(6)° and an intact, non-coordinated aminophenol fragment, which is in agreement with the NMR and IR spectroscopic data for **2**. This Au^I containing building block was then applied as a metalloligand for coordination of the available aminophenol fragment to Ni^{II}. Because of its tendency to form homoleptic species, a **2**/Ni ratio of 2:1 was chosen. Reacting **2** in the presence of 0.5 equivalents of $Ni(NO_3)_2{\cdot}6H_2O$ and NEt_3 in acetonitrile at reflux under aerobic conditions afforded complex **3** as a dark-green solid in 73 % yield (^{31}P NMR: $\delta = 32.92$ ppm; CSI-MS: m/z 1482.2332). Multinuclear NMR spectroscopic data are in agreement with a diamagnetic[9] species in solution, showing symmetry even at low temperatures (220 K). Complex **3** exhibits an intense UV/Vis absorption at 943 nm ($\varepsilon = 17.6 \times 10^3\,M^{-1}\,cm^{-1}$), which is characteristic of the antiferromagnetic coupling of two iminosemiquinonato (isq^-) ligand radicals.[10] Dark-green single crystals suitable for X-ray analysis were obtained by diffusion of pentane into a CH_2Cl_2 solution of **3** (see Figure 2). Most remarkably, the centrosymmetric struc-

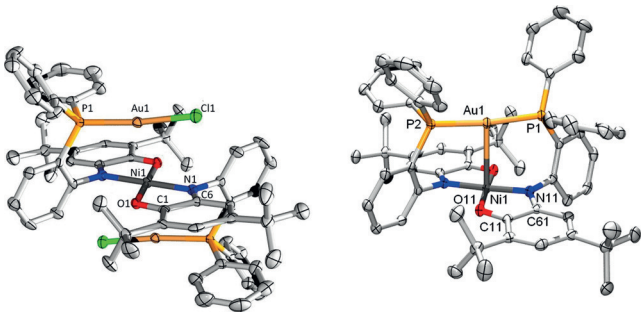

Figure 2. Displacement ellipsoid plots (set at 50 % probability) of **3** (top) and **4** (bottom) at 110(2) K. Hydrogen atoms, counterion (for **4**), and lattice solvent molecules are omitted for clarity. Selected bond lengths [Å] and angles [°] for **3**: Ni1–Au1 3.15862(17), Ni1–O1 1.829(2), Ni1–N1 1.852(2), C6–N1 1.348(4), C1–O1 1.319(4), C1–C6 1.420(4), C1–C2 1.419(5), C2–C3 1.369(4), C3–C4 1.434(5), C4–C5 1.364(5), C5–C6 1.417(4); P1-Au1-Cl1 171.61(3), O1-Ni1-N1 94.40(11). For **4**: Ni1–Au1 2.7429(6), Ni1–O11 1.835(2), Ni1–N11 1.837(3), C61–N11 1.355(4), C11–O11 1.319(4), C11–C61 1.424(4), C11–C21 1.423(4), C21–C31 1.379(5), C31–C41 1.428(5), C41–C51 1.374(5), C51–C61 1.417(4); P1-Au1-P2 173.66(3), O11-Ni1-N11 85.39(11).

ture confirms the presence of an uncommon double d^8–d^{10} interaction[11] in the solid state, as the Ni–Au distance of 3.15857(17) Å is significantly shorter than the sum of their van der Waals radii (3.29 Å). The P1-Au1-Cl1 angle of 171.61(3)° (approx. 5° smaller than in **2**) supports the proposed electronic communication between the central Ni and the peripheral Au atoms. To the best of our knowledge, this is the first complex with a double d^8–d^{10} interaction between Ni and two Au atoms[12] and only the second example of a d^8–d^{10} interaction between Ni and Au.[13] The structure shows characteristic metric parameters for the isq^- oxidation state for both NO fragments (metric oxidation state (MOS) values of -1.13 ± 0.09), confirming the singlet diradical spin state.[9,14] Attempts to abstract a chloride ligand from **3** by using $TlPF_6$ or Ag salts (in MeCN) resulted in the efficient formation of cationic dinuclear AuNi complex **4** (CSI-MS: m/z 1213.3820) as a dark-green diamagnetic solid. Slow evaporation of a diethyl ether/acetonitrile mixture afforded single crystals suitable for X-ray analysis (Figure 2). The molecular structure of the dinuclear species **4** also shows characteristic metric parameters for the isq^- ligand oxidation states (MOS values of -1.13 ± 0.05). A noteworthy observation is the significantly shorter Au–Ni distance (2.7429(6) Å) in **4** than in complex **3** ($\Delta d = -0.4126$ Å).

The metric parameters for **3** and **4** are well-reproduced in the DFT (b3-lyp-d3, def2-TZVP) calculated optimized geometries, with slightly elongated Au–Ni distances found

computationally (see the Supporting Information, Table S1 for a comparison of the metric parameters).[15] The open-shell singlet (OSS) state of **3** is lower in energy than the corresponding closed-shell singlet (CSS) and triplet states by 36.1 and 10.2 kcal mol^{-1}, respectively. Similarly, the OSS state of **4** is lower in energy than the corresponding CSS and triplet states by 12.6 and 20.2 kcal mol^{-1}, respectively. Spin-density plots of the OSS solutions of **3** and **4** (Figure 3, top left and right) illustrate the presence of two ligand-centered radicals. Analysis of the molecular orbitals show weak bonding interactions between a Ni d_{z^2} orbital and a re-hybridized $d_{z^2-x^2}$ orbital on both Au atoms (Figure 3, bottom left and right). In agreement with the shorter Au–Ni distance observed for **4**, a bigger overlap was found for this orbital than for **3**. The filled antibonding orbitals, which are characteristic for $d^{8/10}$–$d^{8/10}$ interactions, were also found at higher energy (see the Supporting Information).

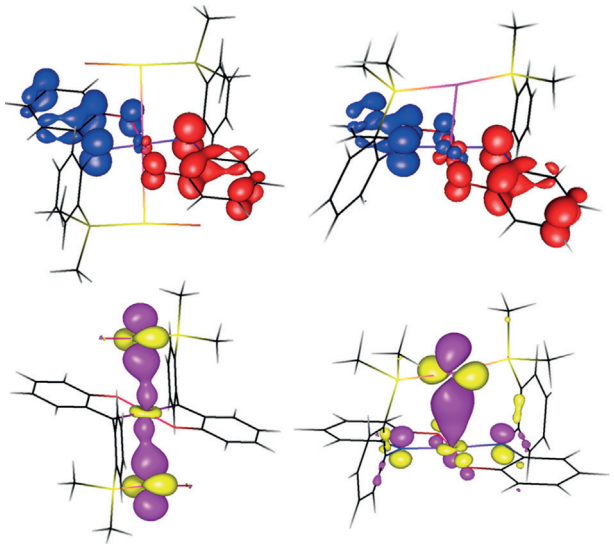

Figure 3. Spin density plots of **3** (OSS; top left) and **4** (OSS; top right) and bonding orbitals of the double d^8–d^{10} interaction in **3** (bottom left, HOMO-23) and the d^8–d^{10} interaction in **4** (bottom right, HOMO-17; b3-lyp-d3, def2-TZVP).

Cyclic voltammetry of **3** in THF shows two reversible reduction events at $E_{1/2}^{red} = -0.68$ V and $E_{1/2}^{red} = -1.50$ V vs. Fc/Fc^+ (Figure 4, red). The reversibility of both reduction events was confirmed by UV/Vis spectroelectrochemistry with an optically transparent thin-layer electrochemical (OTTLE) cell, which showed complete loss of the characteristic interligand charge transfer band at 943 nm upon one-electron reduction to $\mathbf{3}^-$ (see Figure S1). In contrast, a rapid (catalytic) increase in current was observed at the second reduction event in CH_2Cl_2 at −1.4 V vs. Fc/Fc^+, which is indicative of a follow-up reaction with the halogenated solvent and was attributed to C–Cl bond activation (Figure 4, black). Interestingly, several analogous homoleptic $Ni(L^{isq^-})_2$ complexes[8] exhibit well-behaved electrochemistry and do not show any (catalytic) C–Cl bond activation under identical conditions. The former also applies to complex **4**, which shows two fully reversible one-electron reductions

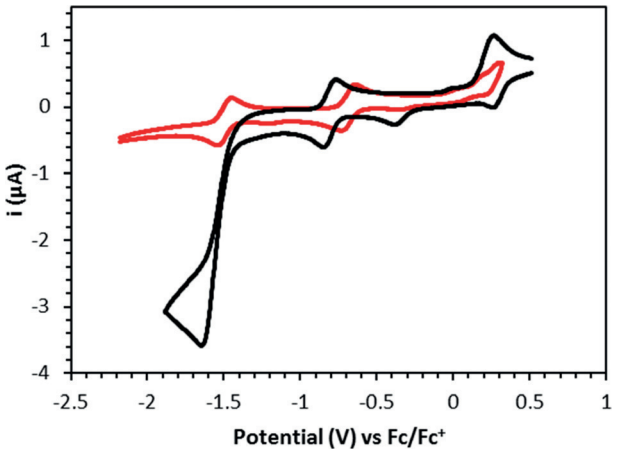

Figure 4. Cyclic voltammograms of **3** (10^{-3} M) recorded in THF (red) and CH_2Cl_2 (black). Scan rate: 100 mV s^{-1}, Pt working electrode, electrolyte: $N(nBu)_4PF_6$ (0.1 M), referenced to Fc/Fc^+.

($E_{1/2}^{red} = -0.80$ V and $E_{1/2}^{red} = -1.55$ V vs. Fc/Fc^+) in CH_2Cl_2 (see Figure S9).

Coordination of the phosphine oxide analogue **5** (see Scheme 2 and the Supporting Information for synthetic details) of ligand **1** to nickel generated the corresponding homoleptic species ($Ni(\mathbf{5}^{isq^-})_2$ (**6**), which shows two reversible one-electron reductions in CH_2Cl_2 (Figure S10) with no sign of dichloromethane C–Cl activation. The absence of catalytic C–Cl activation with both **6** and **4** (with a coordinatively trapped Au) indicates a potential role for the outward-pointing AuCl fragment to induce turnover. The difference in the manner in which the oxidation steps occur for the three $Ni(NO^{isq})_2$ complexes is also suggestive of electronic interactions between the metals and the redox-active ligands. Subtle modulation of the d^8–d^{10} interaction between nickel and gold may be facilitated by the redox-active framework.

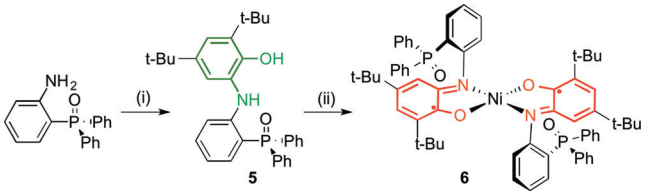

Scheme 2. Synthesis of ligand **5** and homoleptic complex **6**. Reagents and conditions: 3,5-di-*tert*-butylcatechol, AcOH; ii) $NiCl_2 \cdot 6H_2O$, NEt_3, air.

To test the hypothesis of redox-active ligand-through-metal-to-metal electronic communication and follow-up C–X activation, we chose benzyl bromide (BnBr) as a model substrate. The presence of BnBr had a pronounced effect on the intensity of the electrocatalytic wave for the second one-electron reduction in the voltammogram of **2** in THF (Figure 5).[16] Notably, the addition of various amounts of BnBr did not result in a change in the intensity or position of the first one-electron reduction wave. Cyclic voltammetry of a benzyl bromide solution in THF with the same Pt working

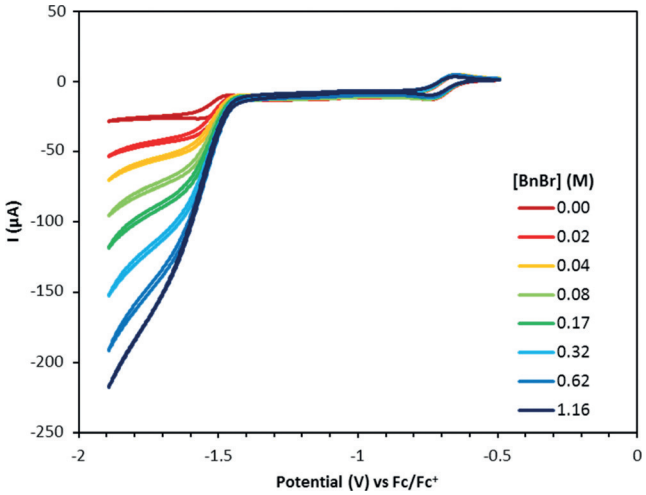

Figure 5. Cyclic voltammograms of **3** recorded in THF (1×10^{-3} M) with increasing [BnBr]. Scan rate: 10 mVs^{-1}, Pt working electrode, electrolyte: $N(nBu)_4PF_6$ (0.1 M), referenced to Fc/Fc^+.

electrode in the absence of **3** only showed the onset of a catalytic current at −2.2 V vs. Fc/Fc^+, which is 0.8 V more negative than with **3**. A linear correlation of i_{cat}/i_p versus [**3**] or [BnBr] (for low substrate concentrations) is observed, whereas saturation behavior is apparent at higher [BnBr] (see the Supporting Information). Cyclic voltammetry in the presence of different *para*-substituted benzyl bromides revealed that electron-withdrawing substituents have a positive effect on the catalytic current, which is in accord with a radical mechanism (see the Supporting Information).[17]

Controlled potential coulometry at −1.5 V vs. Fc/Fc^+ in the presence of 100 equivalents of BnBr produced 1,2-diphenylethane with a TON of approximately 14 and a Faradaic efficiency of 44%. After bulk electrolysis, the dibromide analogue of **3** (**3**-Br_2) was characterized by X-ray analysis of dark single crystals formed upon slow evaporation of the reaction mixture, indicating the generation of bromide ions or bromine atoms upon C–X activation. Cold-spray ionization mass spectrometry (CSI-MS) of the reaction mixture showed fragments derived from **3**-Br with one or two added benzyl groups ($m/z+90$ and $m/z+180$), suggestive of the presence of benzyl radicals. Using an equimolar mixture of BnBr and 4-methylbenzylbromide (4-$MeC_6H_4CH_2Br$) resulted in a statistical mixture of 1,2-diphenylethane, 1-methyl-4-phenethylbenzene, and 1,2-di-*para*-tolylethane. In situ synthesis of the doubly reduced complex by anaerobic deprotonation of **2** in the presence of $Ni(NO_3)_2{\cdot}6H_2O$ followed by addition of solid 4-methylbenzylbromide resulted in the formation of the homocoupled product 1,2-di-*para*-tolylethane, as detected by GC-MS. When the same reaction was performed in the presence of ten equivalents of 2,2,6,6-tetramethyl-1-piperidinyloxy (TEMPO), the formation of the homocoupled product was inhibited and the O-alkylated radical trap was formed, as detected by GC-MS.[18]

In conclusion, we have prepared the unique diamagnetic trinuclear Au^I–Ni^{II}–Au^I complex **3**, which features two antiferromagnetically coupled ligand-centered radicals, as supported by spectroscopic, X-ray diffraction, and computational data. Moreover, the complex features a rare double d^8–d^{10} interaction between the central Ni^{II} and the peripheral Au^I centers. Abstraction of a chloride ligand from the trinuclear complex resulted in the formation of cationic dinuclear Au^I–Ni^{II} complex **4** with a significantly shorter Au–Ni distance. Both complexes show rich electrochemistry, but only the trinuclear complex is able to electrocatalytically convert benzyl bromide into 1,2-diphenylethane upon two-electron reduction, as shown by cyclic voltammetry and controlled potential coulometry experiments. It appears that the nature of the nickel–gold interaction in these heterobimetallic species plays an important role in facilitating electrocatalytic C–C bond formation. Research to elucidate and understand this phenomenon in more detail is in progress.

Experimental Section

CCDC 1429112 (**3**), 1429113 (**3**-Br_2), 1429114 (**4**), and 1429820 (**2**) contain the supplementary crystallographic data for this paper. These data are provided free of charge by The Cambridge Crystallographic Data Centre.

Acknowledgements

This research was funded by the European Research Council through an ERC Starting Grant (*EuReCat*, Grant Agreement 27097) to J.I.v.d.V. We thank Ed Zuidinga for MS analysis, Prof. Dr. Bas de Bruin for useful discussions regarding DFT calculations, and Prof. Dr. Joost Reek for helpful and valuable suggestions.

Keywords: gold · heterobimetallic complexes · metal–metal interactions · nickel · redox-active ligand

How to cite: *Angew. Chem. Int. Ed.* **2016**, *55*, 2406–2410
Angew. Chem. **2016**, *128*, 2452–2456

[1] a) M. L. Crawley, B. M. Trost, *Applications of Transition Metal Catalysis in Drug Discovery and Development: An Industrial Perspective*, Wiley, Hoboken, **2012**; b) M. Beller, C. Bolm, *Transition Metals for Organic Synthesis*, Wiley-VCH, Weinheim, **2008**.

[2] a) D. L. J. Broere, R. Plessius, J. I. van der Vlugt, *Chem. Soc. Rev.* **2015**, *44*, 6886–6915; b) O. R. Luca, R. H. Crabtree, *Chem. Soc. Rev.* **2013**, *42*, 1440–1459; c) V. K. K. Praneeth, M. R. Ringenberg, T. R. Ward, *Angew. Chem. Int. Ed.* **2012**, *51*, 10228–10234; *Angew. Chem.* **2012**, *124*, 10374–10380; d) J. I. van der Vlugt, *Eur. J. Inorg. Chem.* **2012**, 363–375; e) V. Lyaskovskyy, B. de Bruin, *ACS Catal.* **2012**, *2*, 270–279; f) W. Kaim, *Inorg. Chem.* **2011**, *50*, 9752–9765; g) P. J. Chirik, K. Wieghardt, *Science* **2010**, *327*, 794–795.

[3] a) J. L. Wong, R. H. Sánchez, J. C. Logan, R. A. Zarkesh, J. W. Ziller, A. F. Heyduk, *Chem. Sci.* **2013**, *4*, 1906–1910; b) P. J. Chirik in *Pincer and Pincer-type Complexes* (Eds.: K. J. Szabo, O. F. Wendt), Wiley, Hoboken, **2014**, pp. 189–212; c) M.-C. Chang, T. Dann, D. P. Day, M. Lutz, G. G. Wildgoose, E. Otten, *Angew. Chem. Int. Ed.* **2014**, *53*, 4118–4122; *Angew. Chem.* **2014**, *126*, 4202–4206; d) P. J. Chirik, *Acc. Chem. Res.* **2015**, *48*, 1678–1695.

[4] a) D. L. J. Broere, L. L. Metz, B. de Bruin, J. N. H. Reek, M. A. Siegler, J. I. van der Vlugt, *Angew. Chem. Int. Ed.* **2015**, *54*, 1516 – 1520; *Angew. Chem.* **2015**, *127*, 1536 – 1540; b) D. L. J. Broere, B. de Bruin, J. N. H. Reek, M. Lutz, S. Dechert, J. I. van der Vlugt, *J. Am. Chem. Soc.* **2014**, *136*, 11574 – 11577; see also: c) W. Zhou, B. O. Patrick, K. M. Smith, *Chem. Commun.* **2014**, *50*, 9958 – 9960; d) C. A. Lippert, S. A. Arnstein, C. D. Sherill, J. D. Soper, *J. Am. Chem. Soc.* **2010**, *132*, 3879 – 3892.

[5] a) P. Buchwalter, J. Rosé, P. Braunstein, *Chem. Rev.* **2015**, *115*, 28 – 126; b) D. G. H. Hetterscheid, S. H. Chikkali, B. de Bruin, J. N. H. Reek, *ChemCatChem* **2013**, *5*, 2785 – 2793; c) B. G. Cooper, J. W. Napoline, C. M. Thomas, *Catal. Rev. Sci. Eng.* **2012**, *54*, 1 – 40; d) J. Park, H. Sukwon, *Chem. Soc. Rev.* **2012**, *41*, 6931 – 6943; e) N. Wheatley, P. Kalck, *Chem. Rev.* **1999**, *99*, 3379 – 3420.

[6] A. F. Heyduk, D. G. Nocera, *J. Am. Chem. Soc.* **2000**, *122*, 9415 – 9426.

[7] a) T. P. Lin, F. P. Gabbaï, *J. Am. Chem. Soc.* **2012**, *134*, 12230 – 12238; b) J. P. Fackler, *Polyhedron* **1997**, *16*, 1 – 17; c) J. P. Fackler, *Inorg. Chem.* **2002**, *41*, 6959 – 6972.

[8] a) A. Paretzki, M. Bubrin, J. Fiedler, S. Záliš, W. Kaim, *Chem. Eur. J.* **2014**, *20*, 5414 – 5422; b) A. Mukherjee, R. Mukherjee, *Indian J. Chem. Sect. A* **2011**, *50*, 484 – 490; c) P. Chaudhuri, C. N. Verani, E. Bill, E. Bothe, T. Weyhermüller, K. Wieghardt, *J. Am. Chem. Soc.* **2001**, *123*, 2213 – 2223; d) S. Kokatam, T. Weyhermüller, E. Bothe, P. Chaudhuri, K. Wieghardt, *Inorg. Chem.* **2005**, *44*, 3709 – 3717; e) V. Bachler, G. Olbrich, F. Neese, K. Wieghardt, *Inorg. Chem.* **2002**, *41*, 4179 – 4193.

[9] Complex **2** is EPR silent in both solution and the solid state, and magnetic susceptibility measurements showed no magnetic moment.

[10] a) D. Herebian, K. E. Wieghardt, F. Neese, *J. Am. Chem. Soc.* **2003**, *125*, 10997 – 11005; b) K. Chłopek, E. Bothe, F. Neese, T. Weyhermüller, K. Wieghardt, *Inorg. Chem.* **2006**, *45*, 6298 – 6307; c) S. Fuse, H. Tago, M. M. Matiani, Y. Wada, T. Takahashi, *ACS Comb. Sci.* **2012**, *14*, 545 – 550.

[11] a) B. H. Xia, H. X. Zhang, Y. Q. Jiao, Q. J. Pan, Z. S. Li, C. C. Sun, *J. Chem. Phys.* **2004**, *120*, 11487 – 11492; b) B. H. Xia, H. X. Zhang, C. M. Che, K. H. Leung, D. L. Philips, N. Zhu, Z. Y. Zhou, *J. Am. Chem. Soc.* **2003**, *125*, 10362 – 10374; c) O. Crespo, A. Laguna, E. J. Fernández, J. M. López-de-Luzuriaga, P. G. Jones, M. Teichert, M. Monge, P. Pyykkö, N. Runeberg, M. Schütz, H. Werner, *Inorg. Chem.* **2000**, *39*, 4786 – 4792.

[12] For a linear Au–Pt–Au complex, see: H. H. Murray, D. A. Briggs, G. Garzón, R. G. Raptis, L. C. Porter, J. P. Fackler, *Organometallics* **1987**, *6*, 1992 – 1995.

[13] O. Crespo, M. C. Gimeno, A. Laguna, O. Lehtonen, I. Ospino, P. Pyykkö, M. D. Villacampa, *Chem. Eur. J.* **2014**, *20*, 3120 – 3127.

[14] The metric oxidation state (MOS) is a convenient method to determine the oxidation state for aminophenol-related systems; see: S. N. Brown, *Inorg. Chem.* **2012**, *51*, 1251 – 1260.

[15] Dispersion corrections are required to accurately describe the Au – Ni interaction, as reported previously for Pd^{II} – Pd^{II} d^8 – d^8 interactions; see: D. L. J. Broere, S. Demeshko, B. de Bruin, E. A. Pidko, J. N. H. Reek, M. A. Siegler, M. Lutz, J. I. van der Vlugt, *Chem. Eur. J.* **2015**, *21*, 5879 – 5886.

[16] This is similar to what has been reported for a Co^{II} complex containing two redox-active *ortho*-phenylenediamide ligands, although this species is only active at −2.1 V vs. Fc/Fc^+; see: M. van der Meer, Y. Rechkemmer, I. Peremykin, S. Hochloch, J. van Slageren, B. Sarkar, *Chem. Commun.* **2014**, *50*, 11104 – 11106.

[17] a) G. L. Grady, T. J. Danyliw, P. Rabideux, *J. Organomet. Chem.* **1977**, *142*, 67 – 70; b) H. Sakurai, K. Mochida, *J. Organomet. Chem.* **1972**, *42*, 339 – 343; c) L. W. Menapace, M. B. Loewenthal, J. Koscielecki, L. Tucker, L. C. Passaro, R. Montalbano, A. J. Frank, J. Marrantino, J. Brunner, *Organometallics* **2002**, *21*, 3066 – 3068; d) E. V. BlackBurn, D. D. Tanner, *J. Am. Chem. Soc.* **1980**, *102*, 692 – 697; e) C. Chatgilialoglu, K. U. Ingold, J. C. Scaiano, *J. Org. Chem.* **1987**, *52*, 938 – 940; f) D. W. Rogers, A. A. Zavitsas, N. Matsunaga, *J. Phys. Chem. A* **2009**, *113*, 12049 – 12055; g) J. Halpern, P. F. Phelan, *J. Am. Chem. Soc.* **1972**, *94*, 1881 – 1886.

[18] Benzylic radicals are readily trapped by TEMPO; see: a) T. M. Brown, C. J. Cooksey, D. Crich, A. T. Dronsfield, R. Ellis, *J. Chem. Soc. Perkin Trans. 1* **1993**, 2131 – 2136; b) J. Chateauneuf, J. Lusztyk, K. U. Ingold, *J. Org. Chem.* **1988**, *53*, 1629 – 1632; c) A. L. J. Beckwith, V. W. Bowry, K. U. Ingold, *J. Am. Chem. Soc.* **1992**, *114*, 4983 – 4992; d) V. W. Bowry, K. U. Ingold, *J. Am. Chem. Soc.* **1992**, *114*, 4992 – 4996.

Received: October 8, 2015
Revised: December 5, 2015
Published online: January 13, 2016

